Molecular Dynamics Simulations of Glycerol Monooleate Confined between Mica Surfaces

Molecular Dynamics Simulations of Glycerol Monooleate Confined Between Mica Surfaces

Joshua L. Bradley-Shaw,[†] Philip J. Camp,[*,†] Peter J. Dowding,[‡] and Ken Lewtas[†,¶]

School of Chemistry, University of Edinburgh, David Brewster Road, Edinburgh EH9 3FJ, Scotland, Infineum UK Ltd, PO Box 1, Milton Hill, Abingdon OX13 6BB, UK, and Lewtas Science & Technologies, 246 Banbury Road, Oxford OX2 7DY, UK

E-mail: philip.camp@ed.ac.uk

July 13, 2016

[*]To whom correspondence should be addressed
[†]University of Edinburgh
[‡]Infineum UK Ltd
[¶]Lewtas Science & Technologies

Abstract

The structure and frictional properties of glycerol monooleate (GMO) in organic solvents, with and without water impurity, confined and sheared between two mica surfaces are examined using molecular dynamics simulations. The structure of the fluid is characterized in various ways, and the differences between systems with nonaggregated GMO and with preformed GMO reverse micelles are examined. Preformed reverse micelles are metastable under static conditions in all systems. In *n*-heptane under shear conditions, with or without water, preformed GMO reverse micelles remain intact and adsorb on to one or other of the surfaces, becoming surface micelles. In dry toluene, preformed reverse micelles break apart under shear, while in the presence of water, the reverse micelles survive and become surface micelles. In all systems under static and shear conditions, nonaggregated GMO adsorbs on to both surfaces with roughly equal probability. Added water is strongly associated with the GMO, irrespective of shear or the form of the added GMO. In all cases, with increasing shear rate, the GMO molecules flatten on the surface, and the kinetic friction coefficient increases. Under low-shear conditions, the friction is insensitive to the form of the GMO added, while the presence of water is found to lead to a small reduction in friction. Under high-shear conditions, the presence of reverse micelles leads to a significant reduction in friction, while the presence of water increases friction in *n*-heptane and decreases friction in toluene.

1 Introduction

Transportation is one of the largest sectors of the modern economy, but still the effects of friction continue to compromise fuel efficiency, low emissions, and engine lifetime. In order to reduce friction, small concentrations ($\sim$ 1 wt%) of amphiphiles are typically added to a base oil. These surfactant-like molecules are thought to adsorb preferentially on to inorganic surfaces to form a protective layer, where they reduce friction and wear between moving parts, and hence improve fuel economy, reduce emissions, and increase engine lifetime. To date, additive compounds have been developed heuristically as a compromise between the complexity of the molecular chemistry and the efficacy of the lubricant. There is a need to understand – from first principles – how lubricants work, and how they might be optimized. Although lubricants are assessed in large-scale engine tests, this does not offer a viable means of studying lubricants on the molecular scale *in situ*. The critical areas of an engine – such as cam shafts – experience extremely high loads on the order of GPa. Moreover, lubricants contain many chemical components carrying out a variety of roles over and above reducing friction, and isolating the contribution from one component is difficult. The appropriate first step is therefore to study model systems with smooth surfaces and simple lubricant chemistries in order to establish the fundamental molecular-scale processes governing friction. On the experimental side, atomically smooth surfaces such as mica, graphite, and simple metal oxides offer the opportunity to perform quantitative measurements of surfactant-film structure and friction using, e.g., surface force balance (SFB) apparatus,[1–4] polarized neutron reflectrometry, and sum-frequency spectroscopy.[5,6] Neither experiments nor simulations can match all of the experimentally relevant physical conditions in an engine: SFB measurements are limited to low loads and low shear rates; and molecular simulations are limited to very high shear rates and small system sizes. Nonetheless, results in all regimes and from all approaches can help to develop a full description of lubrication and friction.

Systematic experimental studies of friction have primarily focused on the boundary friction regime of the Stribeck curve, that is to say under high loads and with low sliding velocities.[7–11] In this regime, friction is dominated by so-called asperity contacts, where surface features interlock and exert strongly localized stresses. For the most part, experimental studies offer empirical relationships between chemical composition and observed frictional properties. Little can be learned about the detailed microscopic mechanisms connecting molecular-scale structure and dynamics and macroscopic friction, although there are direct measurements of molecular structure under static conditions.[5,6] Molecular dynamics (MD) simulations potentially offer unique insights on the molecular-scale processes that can contribute to the measured friction. Despite ongoing attempts to accelerate computer-simulation approaches,[12] MD simulations are generally limited to the regime of high sliding velocities. Under very high loads, asperity contacts can lead to deformation of the surfaces,[13,14] and avoiding such processes in engines is obviously a priority. The typical surface roughness of engine parts is on the scale of hundreds of nm – much larger than what can be simulated with MD – and so on the atomic scale, the contact zone can be approximated by two parallel surfaces lubricated by a thin fluid layer. In this regime, the roles of the base oil and additives can be explored relatively easily. The presence of a lubricant layer and the application of high sliding velocities correspond to the hydrodynamic friction regime, which has been studied extensively using MD and molecular-mechanics techniques.[15–17] Greenfield and Ohtari studied confined fluids of friction-modifying additives in 1999,[18] and more recently, Davidson *et al.* investigated surface adsorption of organic friction modifiers.[19] MD simulations have been used to study the fundamentals of sliding friction using a variety of simplified molecular models.[20–24] Sliding friction has been studied using fully atomistic models under conditions of constant surface load or separation,[25,26] or constant chemical potential.[27] The surface adsorption and friction of many chemistries have been studied, such as fatty acids and amines,[28–32] glycerin,[33] polymers and hydrocarbons,[34–36] zinc

dithiodialkylphosphates,[37] molybdenum sulfides,[38,39] silanes,[25] and a range of room-temperature ionic liquids.[40,41] The key advantages of simulation are that the structures of surfactants can be examined under shear, and that the frictional properties can be calculated under conditions akin to those at important points in the engine. The transient loads of engine components can be as high as 1 GPa. The local shear rates actually experienced by lubricants and friction modifiers are difficult to estimate, because the surfaces are not atomically smooth; the separations between raised areas on two surfaces can be significantly smaller than the average separation. Even if one reckoned on a minimum surface-surface separation $L_z \sim 10$ nm, and an average sliding velocity $v_s \sim 10$ m s^{-1}, the corresponding local shear rate could be as high as $\dot{\gamma} = v_s/L_z = 10^9$ s^{-1} – immense in engineering terms. The nonequilibrium dynamical properties of simple and complex fluids under such conditions are of considerable inherent interest, and many simulation studies have been devoted to this topic. For example, the shear viscosities of simple alkanes, either in bulk or confined between surfaces, indicate shear thinning at high shear rates.[42,43] Experiments and simulations have been used to demonstrate that when strongly confined between mica surfaces, simple linear alkanes exhibit much higher viscosities than in bulk, and undergo shear thinning at a much lower shear rates than in bulk, related to solid-like ordering and the slowing down of rotational and translational degrees of freedom.[44,45]

This paper is devoted to the study of the structure and frictional properties of GMO – a nonionic surfactant widely used as a friction modifier in engine lubricants – dissolved in the simple solvents *n*-heptane and toluene, and sheared between parallel mica surfaces. The solvents are convenient models of the aliphatic and aromatic components of real base oils. They have approximately the same molecular masses, and similar non-bonded interactions with other atoms, which allow a direct investigation of the effects of solvent molecular architecture. Aside from its use as a friction modifier in engine lubricants, GMO is also used as an emulsifier and antifoaming agent in the

food industry, and as an excipient in pharmaceuticals. The molecular structure of GMO is shown in Figure 1. The effects of GMO on friction have been studied extensively in systems including diamond-like carbon,[46–48] lubricant base stocks,[49] and mixtures with phosphates.[50] GMO is known to self-assemble into normal and reverse micelles (RMs) in aqueous and nonaqueous media, respectively. The self-assembly of GMO and related molecules in hydrocarbons to form RMs has been examined experimentally by Shrestha *et al.*[51–54] The current authors investigated the formation of GMO RMs in *n*-heptane and toluene using MD simulations and small-angle neutron scattering (SANS), with good agreement being found between the two approaches.[55] From that work, it was determined that the typical radius of gyration of a RM is $R_g \simeq 15$ Å, and that the number of GMO molecules in a micelle depends on the solvent and the extent to which it penetrates the RM; there are approximately 20 GMO molecules per RM in toluene, and 30 in *n*-heptane.

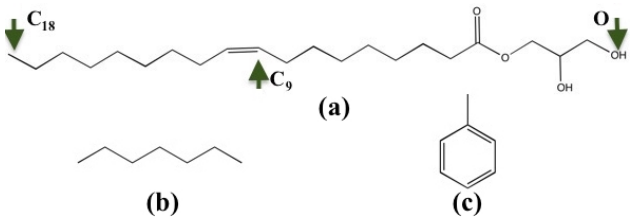

Figure 1: The molecular structures of (a) glycerol monooleate with selected atoms O, C_9, and C_{18} labeled, (b) *n*-heptane, and (c) toluene.

The formation of GMO RMs in bulk organic liquids suggests that the intuitive picture of friction-modifier additives adsorbing on to surfaces to form a protective layer may not always be appropriate. It is therefore important to study the structures adopted by GMO molecules in a lubricant confined between surfaces, and to explore to what extent the GMO and its self-assembled structures modify the measured friction. In this work, mica is used as the model inorganic surface, in order to provide results that could be compared to measurements in future SFB experiments. The SFB apparatus was designed by Tabor and Winterton[1] and developed for application to liquids by Israelachvili and coworkers.[2] The instrument consists of two smooth surfaces, one being attached

to a cantilevered spring which allows the force between the surfaces to be measured. In addition to the force, the distance can also be determined using optical interferometry. Subsequent developments of the technique have allowed the tribological properties of liquids between two surfaces to be measured.[3,4] Mica is often used in SFB measurements as it is possible to achieve atomically smooth surfaces (with an RMS roughness of 1–2 Å). This is a boon from a simulation perspective as surface asperities are difficult to represent explicitly. Despite recent advances in the field, the problems of box size, periodic boundary conditions, and roughness still make surface asperities challenging to describe using MD simulations. Earlier simulation studies of lubricated mica surfaces have focused on structure and dynamics in thin lubricant films,[56] *n*-alkanol monolayers,[57] and surfaces with other hydrophobic coatings.[58]

In this article, the structures of GMO adsorbed on mica are studied under static conditions, and then compared and contrasted with those under shear. Shear rates are studied in the range 10^8–10^{10} s^{-1}. To make connections with previous work, the organic solvent (the 'base oil') is either *n*-heptane or toluene. The article is organized as follows, Section 2 explains the computational methodology used to generate the results presented in Section 3. Section 3.1 contains the results under static conditions, while Section 3.2 gives the results under applied shear. Section 4 concludes the article.

2 Simulation methods

All-atom MD simulations of GMO in either *n*-heptane or toluene, with or without water impurity, and confined between parallel mica surfaces, were performed using LAMMPS.[59,60] In all cases, the equations of motion were integrated with the velocity-Verlet algorithm with a time step of 1 fs. Long-range electrostatic interactions were handled using the Ewald particle-particle particle-mesh method. Essential details are summarized below, and other information such as the parameters and

validation of the force field are given in the Supporting Information.

The basic setup is illustrated in Figure 2. The single-layer mica unit-cell structure (5.1918 Å $\times$ 9.0153 Å $\times$ 10.0228 Å) with stoichiometric aluminum defects was taken from the INTERFACE-PCFF Force Field toolkit.[61–64] The unit cell was tessellated by $10 \times 6 \times 1$ to form a 52 Å $\times$ 54 Å $\times$ 10 Å surface in the *xy* plane. Each mica surface was composed of 2520 atoms. All interatomic interactions were calculated using the INTERFACE-PCFF force field;[61–64] see the Supporting Information for details. The surface was equilibrated under *NPT* conditions for 10^6 timesteps of 1 fs to remove any structural defects that would otherwise cause the surface to warp. The Nosé-Hoover barostat and thermostat were used to maintain the pressure at $P = 1$ atm and the temperature at $T = 298$ K.

Initial fluid configurations with the same *x* and *y* dimensions as the surfaces, and with thicknesses in the range 45–85 Å, were generated using Packmol.[65] The GMO was included either as a preformed RM from a bulk system,[55] or as nonaggregated molecules. Initial configurations were then generated by merging together the configurations of two identical surfaces with the fluid layer in between. System parameters are given in Table 1. The GMO concentration was fixed at around 10 wt%, at which RMs are known to form in bulk.[55] If present, the number of water molecules is the same as the number of GMO molecules, and this comes out to be around 0.5 wt%, which is a typical value for engine lubricants.

The OPLS-AA force field was used in earlier work on GMO in bulk solution.[55] In this work, the INTERFACE-PCFF force field was used for the whole system, including the liquid layer.[61–64] This is because the INTERFACE-PCFF force field is essential for describing the mica surfaces, and it has been optimized for interactions between organic molecules and inorganic surfaces. Moreover, using an internally consistent force field is preferable to generating a hybridized one. To validate the INTERFACE-PCFF force field against earlier work using the OPLS-AA force field,

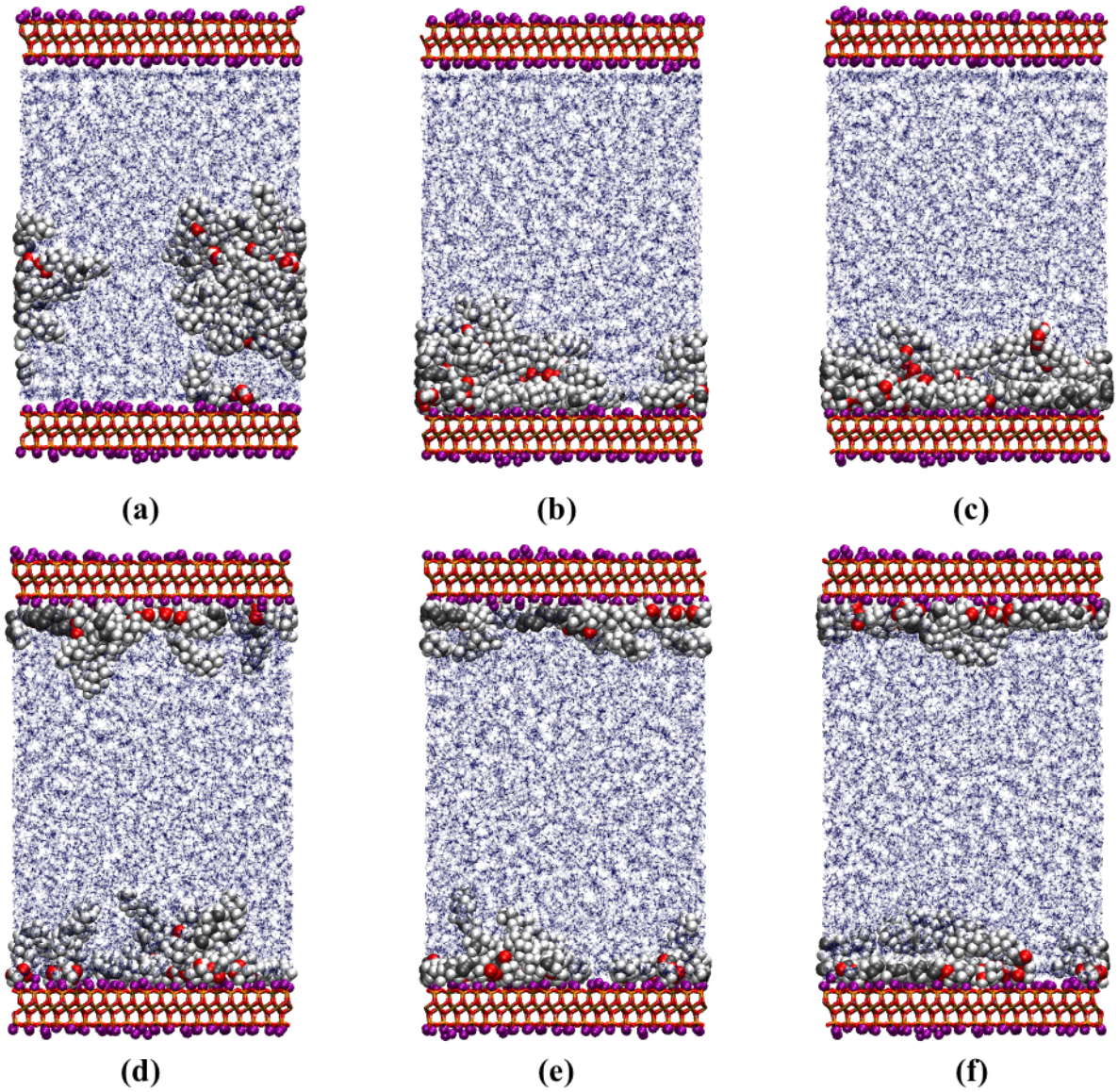

Figure 2: Simulation snapshots of (a)–(c) a preformed GMO RM in *n*-heptane (system H+RM) and (d)–(f) nonaggregated GMO in *n*-heptane (system H). (a) System H+RM under static conditions. (b) System H+RM under low shear $\dot{\gamma} = 1.2 \times 10^9$ s^{-1}. (c) System H+RM under high shear $\dot{\gamma} = 2.5 \times 10^{10}$ s^{-1}. (d) System H under static conditions. (e) System H under low shear $\dot{\gamma} = 1.2 \times 10^9$ s^{-1}. (f) System H under high shear $\dot{\gamma} = 2.5 \times 10^{10}$ s^{-1}. In the mica surfaces, the atom colors are: K (purple); Si (orange); Al (brown); O (red). The *n*-heptane molecules are shown as stick models with C (blue) and H (white). The GMO molecules are shown as space-filling models with C (grey), O (red), and H (white).

Table 1: Details of the system compositions. N_{GMO} is the number of GMO molecules. The solvent is either *n*-heptane (H) or toluene (T). N_{s} is the number of solvent molecules. N_{w} is the number of water (w) molecules. N_{a} is the total number of atoms in the fluid and surfaces. RM (yes/no) shows if a preformed reverse micelle is present. wt%(GMO) and wt%(w) are the weight percentages of GMO and water, respectively. Each system is given a code, e.g., H means *n*-heptane with nonaggregated GMO, and TW+RM means toluene with water and a preformed reverse micelle of GMO.

System	N_{GMO}	Solvent	N_{s}	N_{w}	N_{a}	RM	wt%(GMO)	wt%(w)
H	30	H	961	0	24053	no	10.00	0.00
H+RM	30	H	961	0	24053	yes	10.00	0.00
HW	30	H	956	30	24028	no	9.99	0.50
HW+RM	30	H	956	30	24028	yes	9.99	0.50
T	20	T	696	0	11740	no	10.01	0.00
T+RM	20	T	696	0	11740	yes	10.01	0.00
TW	20	T	693	20	11755	no	10.86	0.55
TW+RM	20	T	693	20	11755	yes	10.86	0.55

and experiment, some tests were done on GMO in bulk solution, and on the pure solvents. The bulk densities of *n*-heptane and toluene at $P = 1$ atm and $T = 298$ K are within 3% of experimental values. With a GMO concentration of 10 wt%, RM formation was observed with both force fields, and the RM dimensions (identified with those of an equivalent ellipsoid of uniform mass density and with the same inertia tensor – see Section 3.1) were practically identical. The detailed results are presented in the Supporting Information.

A constant temperature of $T = 298$ K was maintained with a Nosé-Hoover thermostat. Periodic boundary conditions were applied in the x and y directions. A constant external force was applied to the outermost surface atoms of the upper surface to allow the pressure of the system to be controlled; the z coordinates of the outermost atoms of the lower surface were fixed in space. Typically, an applied pressure of 1000 atm was chosen. The average surface-surface separations under these conditions were $L_z \simeq 70$ Å in *n*-heptane and $L_z \simeq 40$ Å in toluene. From earlier work on bulk GMO in *n*-heptane or toluene, it is known that the diameters of GMO RMs are in the range

25–30 Å.[32] In addition, the *xy* two-dimensional radial distribution functions in similar systems show that the positional correlations between atoms decay over distances of 10–15 Å. Therefore, the dimensions of the fluid layer are just large enough to accommodate the anticipated structures without strong interactions between periodic images and concomitant finite-size effects.

In simulations under static conditions, the system was equilibrated for 1 ns followed by a production run of 5 ns. To apply shear, the outermost atoms of the lower and upper surfaces were given a constant sliding velocity $\pm v_s/2$ in the x direction. The thermostat was applied only in the y direction to ensure that the steady-state velocity profile $v_x(z)$ was not disturbed. Velocities of 2.00, 5.00, 6.25, 10.0, 20.0, 40.0 and 100 m s^{-1} were investigated, giving effective shear rates $\dot{\gamma} = v_s/L_z$ in the range 10^8–10^{10} s^{-1}. The system was equilibrated under static conditions for 1 ns, and then under shear conditions until the velocity profile no longer varied with time and became linear near the center of the fluid layer; this was typically achieved in less than 5 ns. A 5 ns production run under shear conditions was then carried out.

The kinetic friction coefficient μ was calculated using the extended Amontons-Coulomb law $F_L = F_0 + \mu F_N$, where F_L and F_N are the average total lateral (friction) force and normal force (load), respectively, acting on the outermost atoms of each surface, and F_0 is the Derjaguin offset representing the adhesive surface forces.[30] In simulations of similar systems under comparable physical conditions, the Derjaguin offset was $F_0/A \simeq -1$ atm and with a relative error of more than 100%.[31,32] Since the applied load corresponds to a pressure of 1000 atm, the term $\mu F_N \gg F_0$, and hence the kinetic friction coefficient can be approximated by $\mu \simeq F_L/F_N$. This approximation has been tested explicitly in simulations of similar systems, and found to be accurate.[31,32]

3 Results and discussion

Figure 2 shows some simulations snapshots of GMO in *n*-heptane under static conditions, and with low and high shear rates. In Figure 2(a)–(c) the GMO was included as a RM (system H+RM). Under static conditions, the RM remains suspended in the liquid, while under shear conditions, the RM migrates to the surface and adsorbs, flattening in the process. In Figure 2(d)–(f) the nonaggregated GMO molecules adsorb on both surfaces with roughly equal probability. Detailed results will be presented separately for static conditions (section 3.1) and shear conditions (section 3.2).

3.1 Simulations of GMO in *n*-heptane and toluene under static conditions

Systems were first studied under static conditions. The structure of the fluid layer was characterized with mass-density profiles $\rho(z)$, one each for GMO and solvent. Figures 3(a)-(d) and 4(a)-(d) show the mass-density profiles in *n*-heptane and toluene, respectively. The abscissas cover the same range on both sets of graphs for ease of comparison.

In dry solvents, the introduction of nonaggregated GMO molecules [system H – Figure 3(a) – and system T – Figure 4(a)] results in adsorption on to each mica surface with roughly equal probability. The GMO is seen to form a compact layer around 10 Å thick on each surface, and the mass-density profiles for the solvents show significant layering. Preformed GMO RMs in dry solvents [system H+RM – Figure 3(b) – and system T+RM – Figure 4(b)] remain intact and stay largely desorbed from the surfaces. Occasionally, individual GMO molecules dissociated from the RM and adsorbed on to the surfaces, but this is a reversible process.

The positions of added water molecules are dictated by the GMO. The mass-density profiles for nonaggregated GMO in solvents with added water [system HW – Figure 3(c) – and system TW – Figure 4(c)] show that, in these cases, the water adsorbs on to the surfaces along with the GMO, although the distribution is very uneven in case of system TW. When the GMO is added in the

form of a RM [system HW+RM – Figure 3(d) – and system TW+RM – Figure 4(d)] the water is concentrated in the core of the RM.

The dimensions of the RMs have been calculated as outlined in earlier work.[55] Briefly, the inertia tensor of an RM can be calculated by including all GMO molecules belonging to the RM. Then, the dimensions of the RM ($a \leq b \leq c$) are identified with the lengths of the semi-axes of an ellipsoid of uniform mass density, equal mass, and with the same inertia tensor. The radius of gyration R_g can be derived from these dimensions using the formula $R_g^2 = (a^2 + b^2 + c^2)/5$. This is a standard approach to characterize the dimensions of a nonspherical object, and it has been shown to give values of R_g that are consistent with those measured in experiments using SANS.[55] It has also been shown that the interface between the RM and the surrounding solvent is diffuse, and more so in toluene than in *n*-heptane.[55] This was done by calculating radial mass-density profiles of GMO and solvent with respect to the RM center of mass. A diffuse GMO-density profile was incorporated in to the analysis of the SANS data, leading to the aforementioned experimental determination of R_g. The overall consistency between these results shows that the values of a, b, c, and R_g are useful measures of the RM dimensions, despite the RM being a relatively small, molecular-scale object. The results of this analysis are shown in Table 2, along with those measured earlier in simulations of bulk liquids (and corroborated by SANS measurements).[55] There are no systematic differences, except that in dry solvents, the major semi-axis (c axis) decreases upon confinement, while the presence of water is correlated with an increase in c upon confinement.

The orientations of the GMO molecules were examined by calculating various geometrical properties of three selected atoms in each molecule. These atoms are shown in Figure 1(a). Oxygen O is the oxygen of the terminal hydroxyl group, furthest away from the nonpolar tail. Carbon C_9 of the oleate moiety is the double-bonded carbon closest to the head group, and carbon C_{18} is the carbon in the terminal methyl group. The probability distributions of these atoms are noisy due to

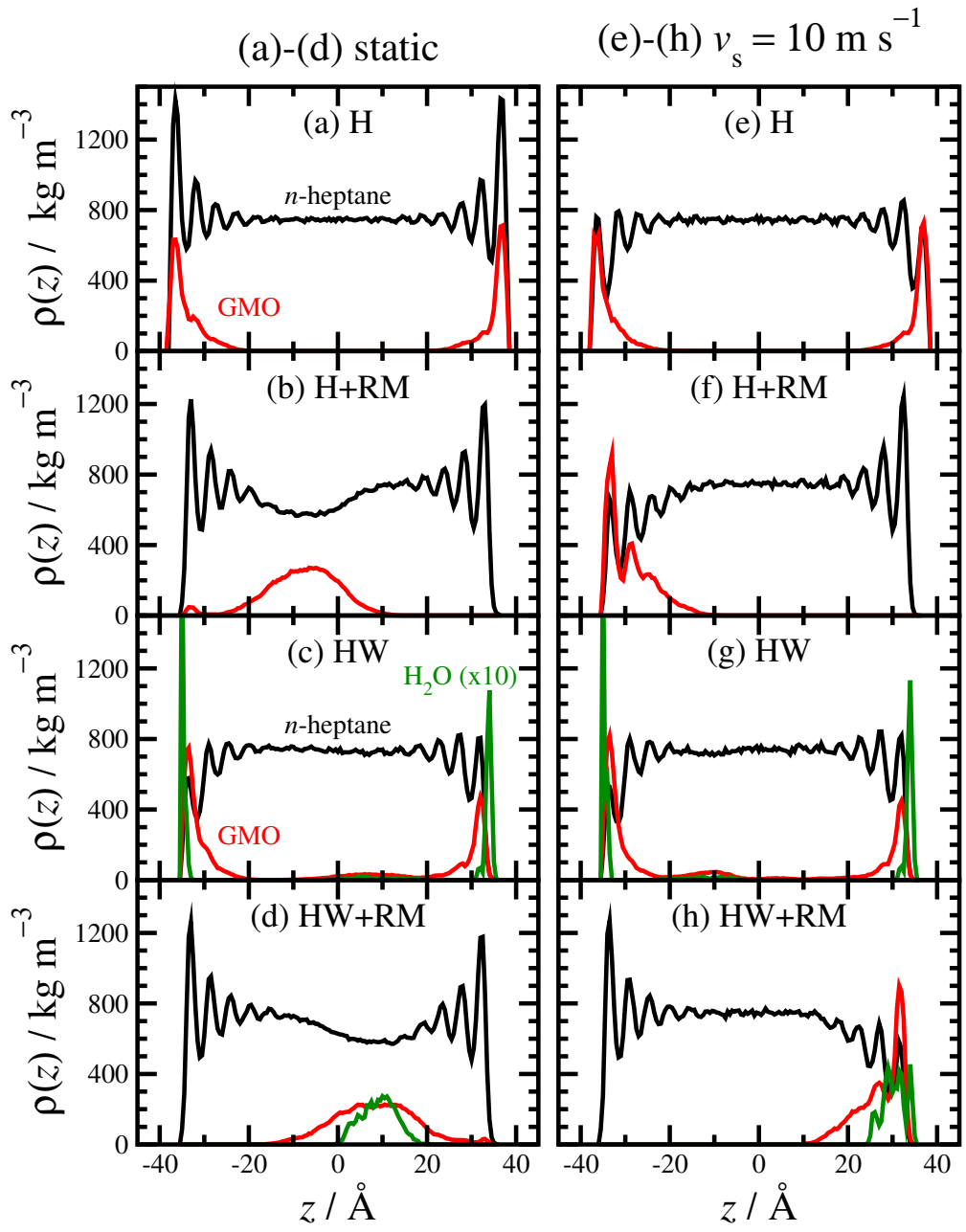

Figure 3: Mass-density profiles $\rho(z)$ in *n*-heptane under static conditions [(a)-(d)] and under shear with sliding velocity $v_s = 10$ m s^{-1} [(e)-(h)]. In (c), (d), (g), and (h), the water densities are multiplied by 10 for clarity.

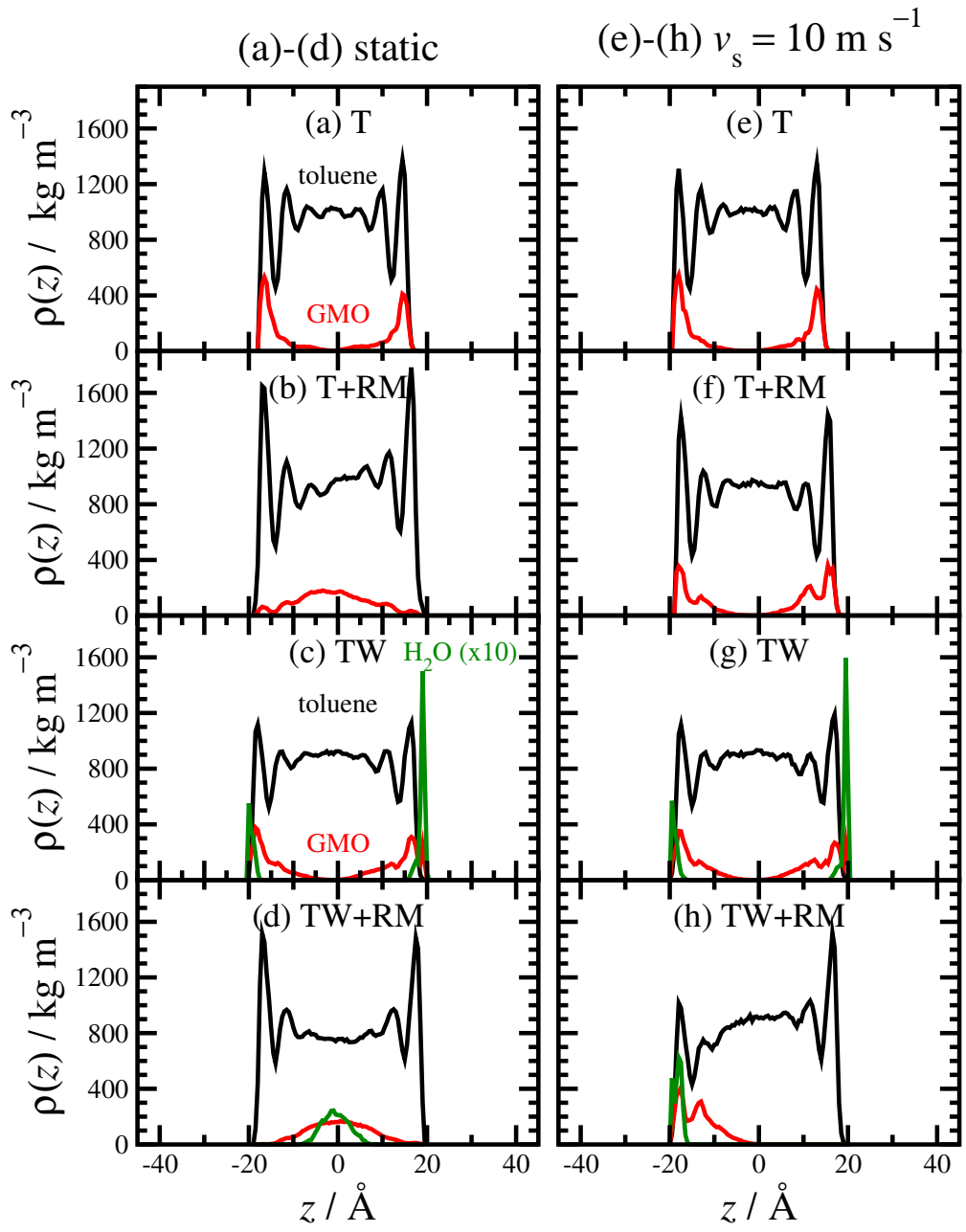

Figure 4: Mass-density profiles $\rho(z)$ in toluene under static conditions [(a)-(d)] and under shear with sliding velocity $v_s = 10$ m s^{-1} [(e)-(h)]. In (c), (d), (g), and (h), the water densities are multiplied by 10 for clarity.

Table 2: Comparison between the dimensions of GMO RMs in bulk liquids[55] and in confined liquids (this work). $a \leq b \leq c$ are the lengths of the semi-axes of an equivalent ellipsoid of uniform mass density, equal mass, and with the same inertia tensor, and R_g is the corresponding radius of gyration.

System	bulk				confined			
	a/Å	b/Å	c/Å	R_g	a/Å	b/Å	c/Å	R_g
H+RM	15.8	18.0	23.1	14.9	16.4	18.0	21.4	14.5
HW+RM	15.2	18.3	23.4	14.9	15.5	20.5	25.0	16.0
T+RM	16.6	20.1	24.7	16.1	13.7	16.3	23.0	14.0
TW+RM	16.0	18.0	20.1	14.0	12.4	16.3	22.9	13.7

the small numbers of GMO molecules: some examples are shown in the Supporting Information. It is clearer to examine some simple statistics, such as the average distances of the atoms from the surface, and the average angles subtended by the atoms and the surface.

The average distances $h(\mathrm{O})$, $h(\mathrm{C}_9)$, and $h(\mathrm{C}_{18})$ of the atoms from the nearest surface are shown (as functions of shear rate) in Figure 5: the results under static conditions are indicated by horizontal dashed lines. In the systems with nonaggregated GMO, which adsorbs on to the surfaces, the O atom is closest to the polar surface, and the C_{18} atom is furthest away. The results for systems T+RM and TW+RM, with preformed RMs and under static conditions, show the opposite ordering because the polar head groups of the GMO molecules are buried inside the desorbed RMs, and the nonpolar tails are pointing outwards towards the surfaces. The same thing happens in systems H+RM and HW+RM, but the results are not shown because the average heights are off the scale at $z \simeq 25$–29 Å. The average positions of the C_{18} atoms in the toluene systems are similar, irrespective of whether the GMO was nonaggregated and adsorbed or in a preformed RM. This is accidental: the wall separation ($L_z \simeq 40$ Å), the radius of gyration of a GMO RM ($R_g \simeq 14$ Å), and the position of the RM just happen to give similar values of $h(\mathrm{C}_{18})$ as in the case of nonaggregated GMO.

To get an idea of the orientation of adsorbed GMO molecules, the average angle between the

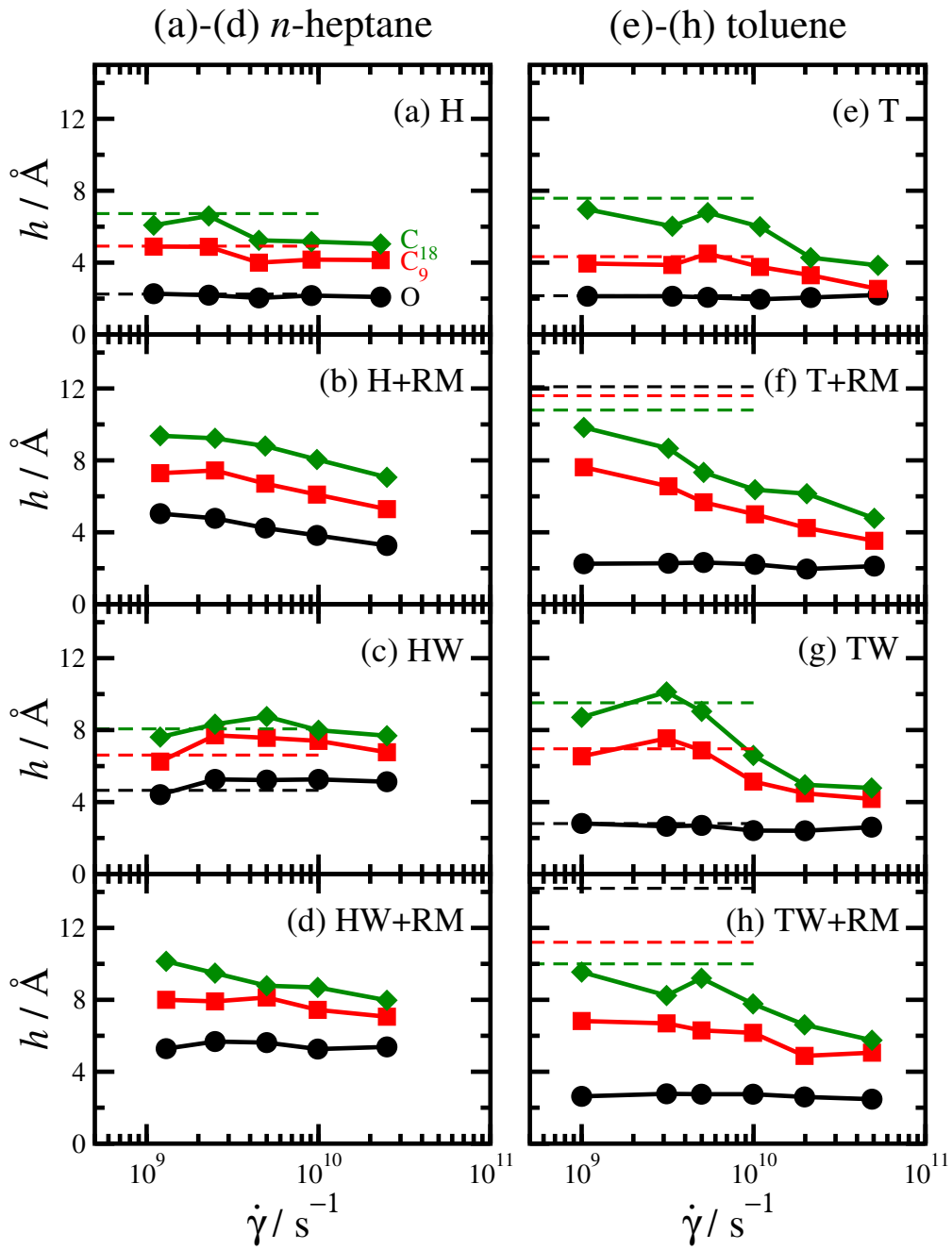

Figure 5: Average heights of selected atoms in GMO from the nearest surface as functions of nominal shear rate $\dot{\gamma} = v_s/L_z$ in *n*-heptane (a)-(d) and toluene (e)-(h): oxygen atom O – black circles; carbon atom C_9 (red squares); carbon atom C_{18} (green diamonds). The dashed lines indicate the average atom heights under static conditions [except for systems H+RM (b) and HW+RM (d) where the atom heights are near the center of the fluid layer at $z \simeq 25$–29 Å].

vector joining atoms O and C_9, and the surface (xy) plane, was calculated. $\theta = 90^\circ$ corresponds to a molecule sitting upright on the surface, while $\theta = 0^\circ$ corresponds to a molecule sitting flat on the surface. It only makes sense to calculate this property for systems with adsorbed, nonaggregated GMO molecules; the results for systems H, HW, T, and TW are shown by the dashed lines in Figure 6. These show that in systems H, HW, and TW, the GMO molecules are anchored on to the surface in a slightly upright orientation ($\theta \simeq 50$–65°). In system T, the GMO molecules are flatter on the surface ($\theta \simeq 20^\circ$) which could be due to packing with neighboring planar toluene molecules that are lying on the surface 'face down'.

3.2 Simulations of GMO in *n*-heptane and toluene under shear conditions

Shear conditions were achieved by specifying a constant sliding velocity $\pm v_s/2$ in the x direction for the surface atoms of the top and bottom surfaces, to achieve a relative sliding velocity of v_s. With a wall separation L_z, this corresponds to a nominal shear rate $\dot{\gamma} = v_s/L_z$. Applied shear in the xz plane sets up a velocity gradient $v_x(z)$. Velocity profiles for *n*-heptane and toluene systems with a sliding velocity $v_s = 10$ m s^{-1} are shown in Figure 7(a) and (b), respectively. In every case, the velocity profile is linear in the middle of the fluid, and the effective shear rate $\dot{\gamma}_{\text{eff}}$ is greater than the nominal one. Near the walls ($z \simeq \pm L_z/2$) there may be layers moving at or near the wall velocity $\pm v_s/2$. These layers are due to molecules and/or RMs adsorbed on the walls. Mass-density profiles under shear conditions in *n*-heptane and toluene are shown in Figures 3(e)-(h) and 4(e)-(h), respectively, and will be discussed in conjunction with the velocity profiles.

The velocity profiles can be analyzed to yield apparent 'stick' lengths at each surface, these being approximately equal to the thicknesses of the adsorbed layers. A schematic diagram of the fitting of the velocity profile is shown in Figure 7(c). In the linear regime, the velocity profile is

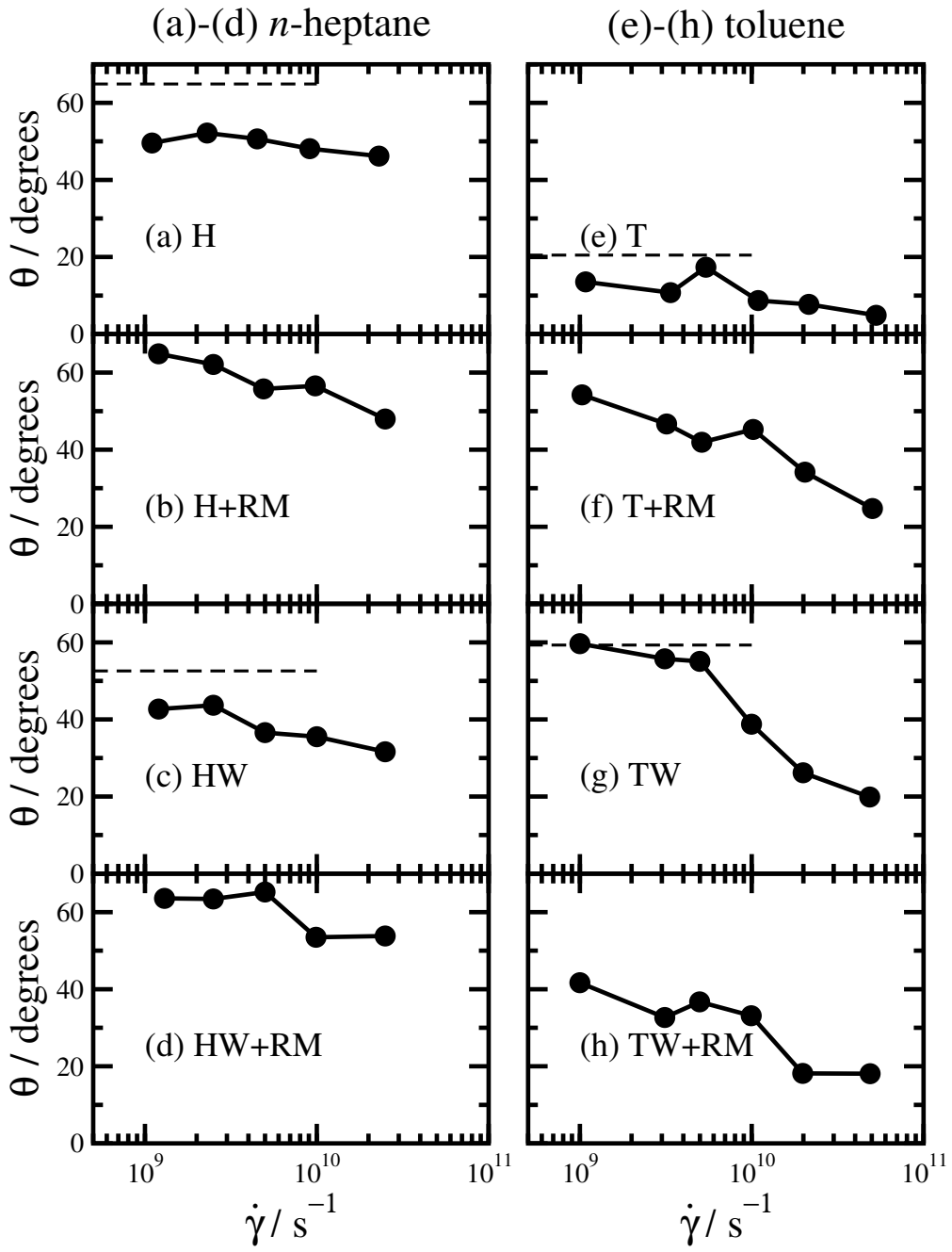

Figure 6: Average angle θ (defined in Section 3.1) in *n*-heptane [(a)-(d)] and toluene [(e)-(h)] with increasing shear rate. In (a), (c), (e), and (g) the dashed lines indicate the average angles under static conditions.

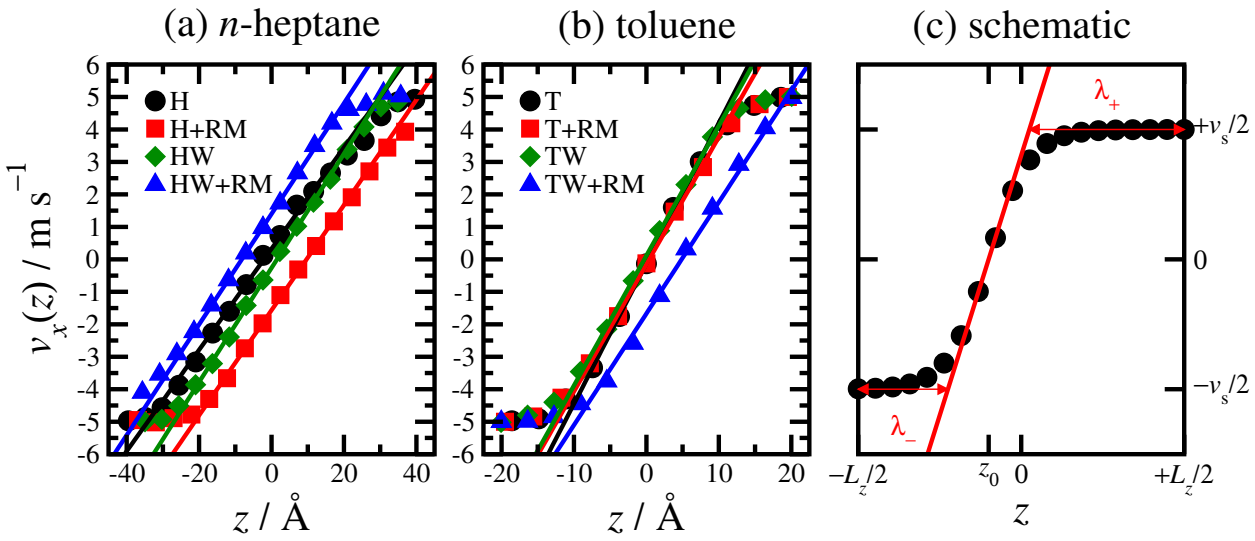

Figure 7: Velocity profiles for systems under shear conditions with sliding velocity $v_s = 10$ m s^{-1}. (a) Systems in *n*-heptane with and without a preformed RM (H+RM and H, respectively). (b) Systems in toluene with and without a preformed RM (T+RM and T, respectively). (c) Schematic diagram of the fitting of the velocity profile: λ_- and λ_+ are the stick lengths at the $z < 0$ ('lower') and $z > 0$ ('upper') surfaces, respectively.

fitted with the equation

$$v_x(z) = \dot{\gamma}_{\text{eff}}(z - z_0) \tag{1}$$

where $\dot{\gamma}_{\text{eff}}$ is the effective shear rate, and $v_x(z_0) = 0$. From the fitted parameters, the apparent stick lengths at the $z < 0$ ('lower') surface (λ_-) and the $z > 0$ ('upper') surface (λ_+) are given by

$$\lambda_\pm = \frac{1}{2}\left(L_z - \frac{v_s}{\dot{\gamma}_{\text{eff}}}\right) \mp z_0. \tag{2}$$

The fits for all systems with $v_s = 10$ s^{-1} are shown in Figure 7(a) and (b), and the fit parameters are given in Table 3.

In *n*-heptane with nonaggregated GMO (systems H and HW) z_0 is very close to the middle of the layer, and λ_- and λ_+ are somewhat similar. The corresponding mass-density profiles in Figure 3(e) and (g) show that the GMO (and water, if present) are adsorbed on both surfaces with roughly

equal probability. The thicknesses of the GMO layers are in the range 5–10 Å, which are in good agreement with $\lambda_{\pm}$. When a GMO RM is added to *n*-heptane, z_0 is almost 10 Å from the middle of the layer. In system H+RM, the stick length at the lower surface is $\lambda_{-} \simeq 16$ Å. Figure 3(f) shows that the GMO RM is adsorbed at the lower surface. In system HW+RM, the stick length at the upper surface is $\lambda_{+} \simeq 15$ Å, and Figure 3(h) shows the GMO and water to be adsorbed on the upper surface. To summarize, in *n*-heptane under shear conditions, nonaggregated GMO adsorbs on to both surfaces with roughly equal probability, while preformed GMO RMs stay intact and adsorb on one surface.

Table 3: Simulation results under shear conditions. L_z is the average wall separation, $\dot{\gamma}_{\rm eff}$ is the effective shear rate, and z_0 is the position of zero velocity in simulations with sliding velocity $v_{\rm s} = 10$ m s^{-1}. λ_{-} and λ_{+} are the corresponding stick lengths in the $z \leq 0$ and $z \geq 0$ layers, respectively [see Figure 7(c) for an illustration]. μ_0 and $\dot{\gamma}_0$ are fit parameters from eq 3 describing the kinetic friction coefficient as a function of the nominal shear rate $\dot{\gamma} = v_{\rm s}/L_z$. $(\mu_0/2\dot{\gamma}_0)$ is the slope of the initially linear increase in μ with $\dot{\gamma}$.

System	L_z/Å	$\dot{\gamma}_{\rm eff}/10^{10}$ s^{-1}	z_0/Å	λ_{-}/Å	λ_{+}/Å	μ_0	$\dot{\gamma}_0/10^{10}$ s^{-1}	$(\mu_0/2\dot{\gamma}_0)/10^{-10}$ s
H	78.6	0.1559 ± 0.0053	-2.11 ± 0.37	5.10 ± 1.1	9.32 ± 1.1	0.113 ± 0.018	0.88 ± 0.19	0.064 ± 0.017
H+RM	73.9	0.1617 ± 0.0020	9.67 ± 0.18	15.69 ± 0.43	-3.64 ± 0.43	0.073 ± 0.017	0.55 ± 0.20	0.066 ± 0.028
HW	71.2	0.1759 ± 0.0030	1.49 ± 0.18	8.65 ± 0.52	5.66 ± 0.52	0.144 ± 0.035	1.15 ± 0.35	0.063 ± 0.025
HW+RM	71.7	0.1703 ± 0.0017	-8.22 ± 0.14	-1.71 ± 0.32	14.73 ± 0.32	0.112 ± 0.025	0.92 ± 0.25	0.061 ± 0.021
T	37.0	0.4325 ± 0.0071	0.289 ± 0.087	7.23 ± 0.21	6.65 ± 0.21	0.1125 ± 0.0056	0.760 ± 0.062	0.0741 ± 0.0071
T+RM	39.1	0.3917 ± 0.0064	0.389 ± 0.091	7.16 ± 0.23	6.39 ± 0.23	0.0944 ± 0.0083	0.626 ± 0.094	0.075 ± 0.013
TW	40.1	0.3999 ± 0.0040	-0.284 ± 0.062	7.25 ± 0.14	7.82 ± 0.14	0.0957 ± 0.0091	0.71 ± 0.11	0.068 ± 0.012
TW+RM	40.2	0.343 ± 0.017	4.87 ± 0.40	10.39 ± 0.84	0.66 ± 0.84	0.0915 ± 0.0046	0.711 ± 0.059	0.0643 ± 0.0062

The mass-density profiles in Figure 4(e) and (g) show that in toluene, nonaggregated GMO molecules adsorb on both surfaces with roughly equal probability. Figure 4(f) shows that a preformed GMO RM in toluene disintegrates under shear conditions. In all of these cases, therefore, one should anticipate a velocity profile with z_0 near to the middle of the layer, and with roughly equal stick lengths at both surfaces. The results in Figure 7(b) and Table 3 bear this out. When a GMO RM is added to toluene with water, though, the RM remains intact and adsorbs on to one of the surfaces, along with the water. Figure 4(h) shows that the RM and water are attached to the lower surface. The results in Figure 7(b) and Table 3 are in agreement, and confirm that the stick length on the lower surface is $\lambda_{-} \simeq 10$ Å.

The calculated friction coefficients μ against the nominal shear rate in *n*-heptane and toluene are given in Figures 8(a) and 8(b), respectively. As has been observed in many situations, μ increases sublinearly with increasing $\dot{\gamma}$ under high-shear conditions. The precise relationship is suspected to be logarithmic.[66–71] As shown explicitly in earlier work,[24,31] an Eyring-like hopping picture leads to the following equation, which accommodates linear behavior at low shear, and logarithmic behavior at high shear:

$$\mu = \mu_0 \ln \left[\frac{\dot{\gamma}}{2\dot{\gamma}_0} + \sqrt{1 + \left(\frac{\dot{\gamma}}{2\dot{\gamma}_0} \right)^2} \right]. \tag{3}$$

Here μ_0 and $\dot{\gamma}_0$ are fitting parameters. At low shear rates ($\dot{\gamma}/2\dot{\gamma}_0 \ll 1$) $\mu \approx \mu_0 \dot{\gamma}/2\dot{\gamma}_0$, while at high shear rates ($\dot{\gamma}/2\dot{\gamma}_0 \gg 1$) $\mu \approx \mu_0 \ln(\dot{\gamma}/\dot{\gamma}_0)$. Hence, there is a crossover from linear to logarithmic behavior at $\dot{\gamma} \sim \dot{\gamma}_0$. Figures 8(a) and (b) show results for *n*-heptane and toluene, respectively, along with fits using eq 3. Figure 8(c) shows all of the results plotted as μ/μ_0 against $\dot{\gamma}/\dot{\gamma}_0$ (on a logarithmic scale), along with the universal curve from eq 3. The fitted curve is found to give an excellent description of the simulated data in every case. The fit parameters are given in Table 3. Note that the variations in the fit parameters are quite small, and moreover the statistical errors are significant. Ideally, a rigorous statistical test would be applied to judge the significance of the variations. This would require sets of independent simulations for each system, and for each shear rate, but these are already demanding calculations, and therefore a proper statistical test is not really feasible. Instead, the following discussion will refer to percentage differences between parameters, indicating trends with structure and composition.

The low-shear behavior is conveniently expressed by the initial linear slope ($\mu_0/2\dot{\gamma}_0$). This is given in Table 3, and it is not very sensitive to whether the GMO is added as an RM or in nonaggregated form, with the percentage changes being not more than 4%. The addition of water leads

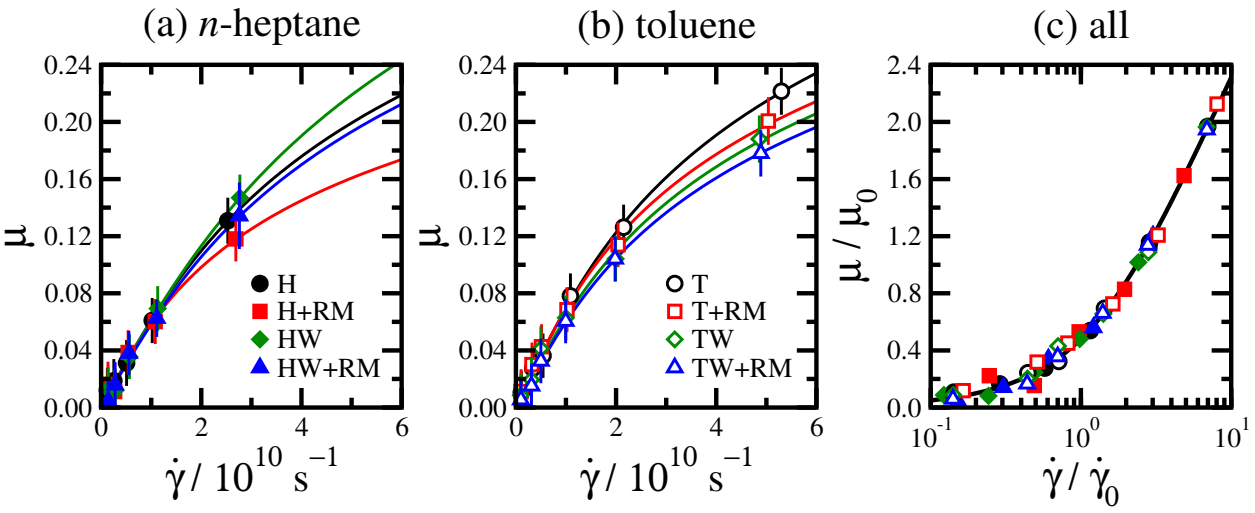

Figure 8: Kinetic friction coefficients μ as a function of the nominal shear rate $\dot{\gamma} = v_s/L_z$ in (a) *n*-heptane and (b) toluene. In (c) all of the data are shown on a universal plot of μ/μ_0 against $\dot{\gamma}/\dot{\gamma}_0$, where μ_0 and $\dot{\gamma}_0$ are fit parameters in eq 3.

to a small but systematic decrease in friction in the low-shear regime. The percentage decreases in $(\mu_0/2\dot{\gamma}_0)$ are -2% [systems H(W)], -8% [systems H(W)+RM], -9% [systems T(W)], and -15% [systems T(W)+RM]. This could be due to the strongly adsorbed water layers – shown in Figures 3 and 4 – lubricating the surfaces. Very thin layers of water confined between mica surfaces remain fluid due to their high rotational and translational mobilities,[72] to be contrasted with the behavior of alkanes which can show solid-like ordering.[45,73] Phosphoric acid confined between silica surfaces undergoes polymerization at high temperature, leading to the production of water, a reduction in the number of hydrogen bonds between acid molecules, and a reduction in friction.[74] The correlation between hydrogen bonding and friction has been observed in other systems: for example, the friction between peptides and hydroxylated surfaces is proportional to the number of hydrogen bonds, and statistical theories have been constructed to explain the observed behavior.[75]

Figure 8(a) and (b) show that at high shear rates, the systems with preformed RMs have lower friction coefficients than those with nonaggregated GMO. This is reflected in the values of μ_0

in Table 3, which dictates the friction in the high-shear regime. The percentage decreases in μ_0 are -35% [systems H(+RM)], -22% [systems HW(+RM)], -16% [systems T(+RM)], and -4% [systems TW(+RM)]. The main difference between the systems in *n*-heptane is that nonaggregated GMO forms layers on both surfaces while a preformed RM flattens on one surface only. This suggests that one high surface-coverage layer of GMO reduces friction better than two sparse ones: a sparse, strongly adsorbed layer of GMO cannot provide a soft interface between the solvent and the hard surface to reduce friction. The systems in toluene do not show such a strong effect, probably because there are fewer GMO molecules per surface, and consequently both types of film are sparse. The addition of water increases the fitted values of μ_0 in systems H(W) ($+27\%$) and H(W)+RM ($+53\%$), while the opposite is true in systems T(W) (-16%) and T(W)+RM (-3%). In the case of *n*-heptane, this could be due to the coordination of water and the polar head groups of GMO at the mica surface, leading to the GMO films becoming more structured and rigid: the density profiles in Figure 3(e)–(h) show that the water is always strongly correlated with the GMO. In system TW, Figure 4(f) shows that most of the water is on one surface, while the GMO is distributed between two, and so the single thick water layer could be the cause of the small drop in friction as compared to system T. The difference in μ_0 between systems TW and TW+RM is too small to rationalize.

As an aside, simulations of pure solvents at shear rates of $\dot{\gamma} \simeq 0.5 \times 10^{10}$ s^{-1} and the same wall separations yield practically identical friction coefficients to those with GMO, within the statistical uncertainties (shown for the latter in Figure 8). Crucially, though, in the pure solvents, the lengths $\lambda_\pm$ are negative ($\lambda_+ = \lambda_- \simeq -8$ Å and -1 Å in *n*-heptane and toluene, respectively) meaning that there are slip planes at the interfaces between the solvent and the hard surfaces, and $\dot{\gamma}_{\text{eff}} < \dot{\gamma}$. In the systems with GMO, the surface-adsorbed molecules reduce the effective thickness of the solvent layer, and enhance the effective shear rate (leading to the values of $\dot{\gamma}_{\text{eff}} > \dot{\gamma}$ shown in Table 3) and

yet the friction coefficients remain practically the same. This shows the friction-reducing effect of the soft interface between GMO and solvent, which offsets the increase in friction that arises from an increased effective shear rate. Figure 8 shows that at shear rates $\dot{\gamma} \sim 10^{10}$ s^{-1}, the friction coefficient $\mu \simeq 0.06$–0.08. Even at lower shear rates ($\dot{\gamma} \sim 10^{9}$ s^{-1}) the friction coefficients of stearic acid and oleic acid in squalane ($\mu \simeq 0.25$)[31] and hexadecylamine in dodecane ($\mu \simeq 0.08$)[32] are higher. At least one contributing factor here is that *n*-heptane and toluene have lower viscosities than dodecane and squalane.

As under static conditions, the heights of selected atoms in the GMO molecule (O, C_9, and C_{18}) are useful in characterizing the molecular conformations near the surfaces. The average heights of these atoms as functions of nominal shear rate in both *n*-heptane and toluene are shown in Figure 5. In all cases, the hydroxyl-group oxygen O is closest to the surface, followed by C_9 and then C_{18}. In most cases, the heights decrease with increasing shear rate, showing how the GMO molecules – either nonaggregated or in an RM – flatten on the surface. The extent of this decrease appears greater in the toluene systems, although because the wall separations are smaller in these cases, higher nominal and effective shear rates have been reached at the highest sliding velocities. Another possible explanation is that toluene is less structured near the surfaces (compare Figures 3 and 4) meaning that the GMO molecules are freer to flatten in the shear flow. In toluene, the methyl C_9 and alkene C_{18} GMO atoms show reductions of up to 50% in the distance from the surface under shear, compared to the hydroxyl O atom, which exhibits a reduction of less than 10%. In *n*-heptane, the atoms in a GMO RM generally have higher average heights than those in nonaggregated GMO, showing that the inherent structure of the RM stops the atoms from coming in close contact with the surface. It was shown in earlier work that *n*-heptane penetrates the RM less than does toluene, and so the average GMO concentration in an RM should be higher.[55] In all systems, the presence of water results in greater average GMO-atom heights than the corresponding

systems without water. This shows that water is preferentially adsorbed to the surface and shielded from the hydrophobic solvent by the GMO surfactant. The mass-density profiles in Figures 3 and 4 show the same effects.

The change in conformation of the GMO molecules with increasing shear rate is examined further with the angle θ defined in Section 3.1. θ is shown as a function of nominal shear rate for each system in Figure 6. As expected, θ decreases with increasing shear rate as the molecules flatten on the surface. In *n*-heptane, the average angle is greater for systems with a GMO RM, showing that the greater packing of the GMO molecules in this situation leads to them 'sitting up' more than the more disperse, nonaggregated GMO molecules. Comparing systems H and HW, the average height of the C_9 atoms increases by 2–3 Å upon addition of water [Figure 5(a) and (c)] while the angle decreases by about 10° [Figure 6(a) and (c)] and should lead to the C_9 atoms being closer to the surface ($h \sim \sin\theta$). This isn't a contradiction: the angle effect is very small because $\sin\theta$ decreases by only 20%, and this is outweighed by the water-layer effect. As shown by the analysis of atomic heights, the angles show that the GMO molecules in toluene flatten more than in *n*-heptane, reflecting the higher shear rates and/or lower surface coverages.

The snapshots in Figure 2 and the mass-density profiles in Figures 3 and 4 show that GMO RMs can be at least metastable under both static and shear conditions, and that they can adsorb on to a surface. To investigate the stability of a surface RM, a significantly larger mica surface was constructed with dimensions of 110×116Å, and the surface micelle of 30 GMO was placed in the middle of this surface in *n*-heptane at 5 wt%. The system contained approximately 66000 atoms (as shown in the Table of Contents graphic) and was run under static conditions for 16 ns over 32 processors on a beowulf cluster. Snapshots of the RM at the start and the end of the simulation are shown in Figure 9. These show that the RM remains intact, although one GMO molecule diffused from the surface micelle to the other surface during the simulation. It could

be that forming a micelle from free GMO on a surface is beyond the simulation timescale, due to a more rapid initial physisorption of GMO on the surface, or perhaps a different number of molecules are needed to form a surface RM. Notwithstanding this, it is suggested that beyond the critical micelle concentration (CMC, estimated to be ~ 0.1 wt%) surface RMs of GMO are expected to survive under shear, whereas below the CMC, only limited aggregation will occur.

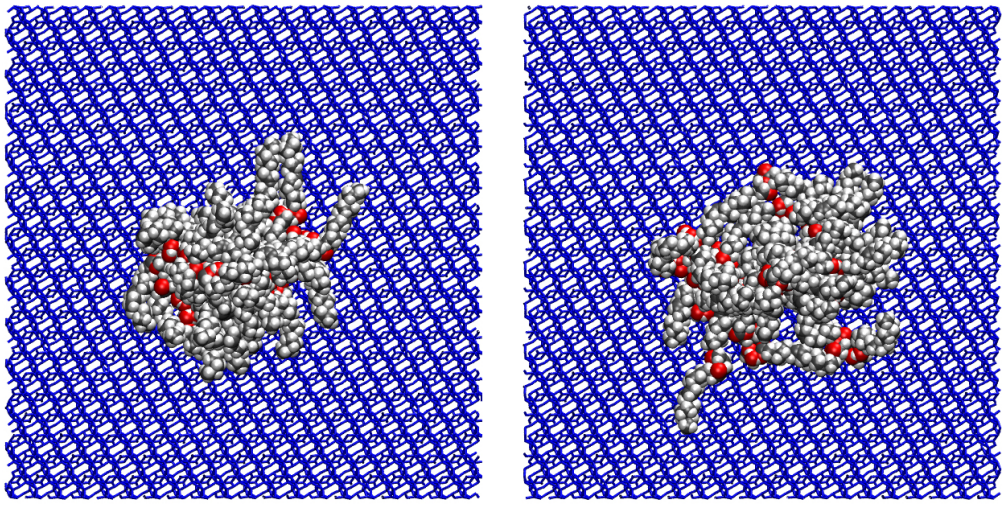

(a) start **(b) end**

Figure 9: Simulation snapshots of a GMO RM on a surface at the start (a) and the end (b) of a 16 ns simulation.

4 Conclusions

In this work, MD simulations of GMO in *n*-heptane and toluene solvents confined between mica surfaces were studied to elucidate structural and frictional properties. It was shown that under static conditions, nonaggregated GMO molecules adsorb onto both mica surfaces with roughly equal probability, while preformed GMO RMs remain desorbed. The presence of water does not affect the structures of these systems significantly.

Under shear conditions, all systems show strong adsorption of GMO onto the mica surfaces. A preformed GMO RM in *n*-heptane (with or without water) adsorbs on to one surface and remains intact. In dry toluene, preformed GMO RMs disintegrate and the molecules adsorb on to both surfaces with roughly equal probability, while in the presence of water, the GMO RM remains intact and adsorbs on to one surface. With increasing shear rate, the GMO molecules (whether nonaggregated or in a RM) flatten on the surface.

At the lower shear rates simulated, the friction coefficient itself does not vary significantly between different systems. The initial linear slope of the friction coefficient, extracted from fitted parameters, indicates that friction is reduced slightly by the presence of water, pointing to a lubricating role for adsorbed water molecules. The slope is not very sensitive to whether GMO is added in nonaggregated form or as a preformed RM.

At the higher shear rates simulated, the presence of a RM can have a significant effect on friction. In *n*-heptane, a reduction in friction is correlated with the adsorption of GMO on a single surface, as happens with the addition of a preformed RM; nonaggregated GMO adsorbs on both surfaces with equal probabilities. A single thick layer of GMO appears to reduce friction more than two thin ones. The situation is not so clear in toluene, probably because the surface coverages are lower, and so both types of film are thin. The presence of water increases the high-shear friction in *n*-heptane significantly, possibly due to a structuring effect of the GMO layer by water molecules at the surface. Again, the situation in toluene is not very clear, but water appears to reduce the friction slightly.

Overall, the effects of solvent, GMO aggregates, and water on friction are quite weak under low-shear conditions, but water consistently reduces friction. Under high-shear conditions, the presence of RMs consistently reduces friction, while the effects of added water depend on solvent and GMO surface coverage. The spatial distribution of GMO on the surfaces could also affect

chemical corrosion and wear. Detailed *ab-initio* MD simulations on the required lengthscales and timescales to study corrosion and wear are not yet feasible.

Associated Content

Supporting Information Available: This material is divided up in to the following sections: (1) Molecular dynamics simulation parameters; (2) INTERFACE-PCFF parameters; (3) Comparison between the OPLS-AA and INTERFACE-PCFF force fields; (4) GMO atom-height distributions. This material is available free of charge via the Internet at `http://pubs.acs.org`.

Acknowledgement

J. L. B.-S. thanks Infineum UK Ltd for the award of a PhD studentship, and Dr Michael Doig and Julien Sindt for helpful discussions.

References

(1) Tabor, D.; Winterton, R. H. S. The Direct Measurement of Normal and Retarded van der Waals Forces. *Proc. R. Soc. Lond. A.* **1969**, *312*, 435–450.

(2) Israelachvili, J. N.; Adams, G. E. Measurement of Forces Between Two Mica Surfaces in Aqueous Electrolyte Solutions in the Range 0-100 nm. *J. Chem. Soc., Faraday Trans. 1* **1978**, *74*, 975–1001.

(3) Direct Measurement of Structural Forces Between Two Surfaces in a Nonpolar Liquid. *J. Chem. Phys.* **1981**, *75*, 1400–1411.

(4) Kumacheva, E.; Klein, J. Simple Liquids Confined to Molecularly Thin Layers. II. Shear and Frictional Behavior of Solidified Films. *J. Chem. Phys.* **1998**, *108*, 7010–7022.

(5) Campana, M.; Teichert, A.; Clarke, S.; Steitz, R.; Webster, J. R. P.; Zarbakhsh, A. Surfactant Adsorption at the Metal-Oil Interface. *Langmuir* **2011**, *27*, 6085–6090.

(6) Wood, M. H.; Welbourn, R. J. L.; Charlton, T.; Zarbakhsh, A.; Casford, M. T.; Clarke, S. M. Hexadecylamine Adsorption at the Iron Oxide-Oil Interface. *Langmuir* **2013**, *29*, 13735–13742.

(7) Hardy, W.; Bircumshaw, I. Boundary Lubrication. Plane Surfaces and the Limitations of Amontons' Law. *Proc. R. Soc. Lond. A* **1925**, *108*, 1–27.

(8) Yoshizawa, H.; Chen, Y. L.; Israelachvili, J. Fundamental Mechanisms of Interfacial Friction. 1. Relation between Adhesion and Friction. *J. Phys. Chem.* **1993**, *97*, 4128–4140.

(9) Bliznyuk, V. N.; Everson, M. P.; Tsukruk, V. V. Nanotribological Properties of Organic Boundary Lubricants: Langmuir Films Versus Self-Assembled Monolayers. *J. Tribol.* **1998**, *120*, 489–495.

(10) Pettersson, U.; Jacobson, S. Influence of Surface Texture on Boundary Lubricated Sliding Contacts. *Tribol. Int.* **2003**, *36*, 857–864.

(11) Pettersson, U.; Jacobson, S. Friction and Wear Properties of Micro Textured DLC Coated Surfaces in Boundary Lubricated Sliding. *Tribol. Lett.* **2004**, *17*, 553–559.

(12) Martini, A.; Dong, Y.; Perez, D.; Voter, A. F. Low-Speed Atomistic Simulation of Stick-Slip Friction using Parallel Replica Dynamics. *Tribol. Lett.* **2009**, *36*, 63–68.

(13) Zheng, X.; Zhu, H.; Kosasih, B.; Tieu, A. K. A Molecular Dynamics Simulation of Boundary Lubrication: The Effect of *n*-Alkanes Chain Length and Normal Load. *Wear* **2013**, *301*, 62–69.

(14) Zhu, H. T.; Zheng, X.; Kosasih, P. B.; Tieu, A. K. Tribo-Surface Charge and Polar Lubricant Molecules on Friction and Lubrication Under Multiple 3D Asperity Contacts. *Wear* **2015**, *332-333*, 1248–1255.

(15) Gao, J.; Luedtke, W. D.; Landman, U. Friction Control in Thin-Film Lubrication. *J. Phys. Chem. B* **1998**, *102*, 5033–5037.

(16) Kamei, D.; Zhou, H.; Suzuki, K.; Konno, K.; Takami, S.; Kubo, M.; Miyamoto, A. Computational Chemistry Study on the Dynamics of Lubricant Molecules under Shear Conditions. *Tribol. Int.* **2003**, *36*, 297–303.

(17) Saito, Y.; Sasaki, N.; Komatsu, T. Molecular Dynamics Simulation for Lubricant Shear Properties During Heating. *IEEE Trans. Magn.* **2012**, *48*, 2009–2015.

(18) Greenfield, M. L.; Ohtani, H. Molecular Dynamics Simulation Study of Model Friction Modifier Additives Confined Between Two Surfaces. *Tribol. Lett.* **1999**, *7*, 137–145.

(19) Davidson, J. E.; Hinchley, S. L.; Harris, S. G.; Parkin, A.; Parsons, S.; Tasker, P. A. Molecular Dynamics Simulations to Aid the Rational Design of Organic Friction Modifiers. *J. Mol. Graphics Modell.* **2006**, *25*, 495–506.

(20) Thompson, P. A.; Robbins, M. O. Shear-Flow Near Solids - Epitaxial Order and Flow Boundary-Conditions. *Phys. Rev. A* **1990**, *41*, 6830–6837.

(21) He, G.; Robbins, M. O. Simulations of the Kinetic Friction Due to Adsorbed Surface Layers. *Tribol. Lett.* **2001**, *10*, 7–14.

(22) He, G.; Robbins, M. O. Simulations of the Static Friction Due to Adsorbed Molecules. *Phys. Rev. B* **2001**, *64*, 035413.

(23) Müser, M. H.; Urbakh, M.; Robbins, M. O. Statistical Mechanics of Static and Low-Velocity Kinetic Friction. *Adv. Chem. Phys.* **2003**, *126*, 187–272.

(24) Farrow, M. R.; Chremos, A.; Camp, P. J.; Harris, S. G.; Watts, R. F. Molecular Simulations of Friction Modification in Nanoscale Fluid Layers. *Tribol. Lett.* **2011**, *42*, 325–337.

(25) Rivera, J. L.; Jennings, G. K.; McCabe, C. Examining the Frictional Forces Between Mixed Hydrophobic-Hydrophilic Alkylsilane Monolayers. *J. Chem. Phys.* **2012**, *136*, 244701.

(26) Hoang, H.; Galliero, G. Shear Behavior of a Confined Thin Film: Influence of the Molecular Dynamics Scheme Employed. *J. Chem. Phys.* **2013**, *138*, 054707.

(27) Elliott, I. G.; Kuhl, T. L.; Faller, R. A Molecular Dynamics Technique to Extract Forces in Soft Matter Systems Under Compression With Constant Solvent Chemical Potential. *J. Chem. Theory Comput.* **2012**, *8*, 1072–1077.

(28) Lundgren, S. M.; Ruths, M.; Danerlöv, K.; Persson, K. Effects of Unsaturation on Film Structure and Friction of Fatty Acids in a Model Base Oil. *J. Colloid Interface Sci.* **2008**, *326*, 530–536.

(29) Ruths, M.; Lundgren, S.; Danerlöv, K.; Persson, K. Friction of Fatty Acids in Nanometer-Sized Contacts of Different Adhesive Strength. *Langmuir* **2008**, *24*, 1509–1516.

(30) Eder, S.; Vernes, A.; Betz, G. On the Derjaguin Offset in Boundary-Lubricated Nanotribological Systems. *Langmuir* **2013**, *29*, 13760–13772.

(31) Doig, M.; Warrens, C. P.; Camp, P. J. Structure and Friction of Stearic Acid and Oleic Acid Films Adsorbed on Iron-Oxide Surfaces in Squalane. *Langmuir* **2014**, *30*, 186–195.

(32) Doig, M.; Camp, P. J. The Structures of Hexadecylamine Films Adsorbed on Iron-Oxide Surfaces in Dodecane and Hexadecane. *Phys. Chem. Chem. Phys.* **2015**, *17*, 5248–5255.

(33) Morita, Y.; Jinno, S.; Murakami, M.; Hatakeyama, N.; Miyamoto, A. A Computational Chemistry Approach for Friction Reduction of Automotive Engines. *Int. J. Engine Res.* **2014**, *15*, 399–405.

(34) Sivebaek, I. M.; Samoilov, V. N.; Persson, B. N. J. Velocity Dependence of Friction of Confined Hydrocarbons. *Langmuir* **2010**, *26*, 8721–8728.

(35) Sivebaek, I. M.; Samoilov, V. N.; Persson, B. N. J. Effective Viscosity of Confined Hydrocarbons. *Phys. Rev. Lett.* **2012**, *108*, 036102.

(36) Zheng, X.; Zhu, H.; Tieu, A. K.; Chen, K. Molecular Dynamics Simulation of Confined *n*-Alkanes: Ordered Structure and Crystalline Bridges. *Int. J. Surface Science and Engineering* **2014**, *8*, 201–212.

(37) Berro, H.; Fillot, N.; Vergne, P. Molecular Dynamics Simulation of Surface Energy and ZDDP Effects on Friction in Nano-Scale Lubricated Contacts. *Tribol. Int.* **2010**, *43*, 1811–1822.

(38) Onodera, T.; Morita, Y.; Suzuki, A.; Koyama, M.; Tsuboi, H.; Hatakeyama, N.; Endou, A.; Takaba, H.; Kubo, M.; Dassenoy, F.; Minfray, C.; Joly-Pottuz, L.; Martin, J.-M.; Miyamoto, A. A Computational Chemistry Study on Friction of h-MoS_2. Part I. Mechanism of Single Sheet Lubrication. *J. Phys. Chem. B* **2009**, *113*, 16526–16536.

(39) Onodera, T.; Morita, Y.; Nagumo, R.; Miura, R.; Suzuki, A.; Tsuboi, H.; Hatakeyama, N.; Endou, A.; Takaba, H.; Dassenoy, F.; Minfray, C.; Joly-Pottuz, L.; Kubo, M.; Martin, J.-

M.; Miyamoto, A. A Computational Chemistry Study on Friction of h-MoS_2 Part II. Friction Anisotropy. *J. Phys. Chem. B* **2010**, *114*, 15832–15838.

(40) Canova, F. F.; Matsubara, H.; Mizukami, M.; Kurihara, K.; Shluger, A. L. Shear Dynamics of Nanoconfined Ionic Liquids. *Phys. Chem. Chem. Phys.* **2014**, *16*, 8247–8256.

(41) Mendonça, A. C. F.; Pádua, A. A. H.; Malfreyt, P. Nonequilibrium Molecular Simulations of New Ionic Lubricants at Metallic Surfaces: Prediction of the Friction. *J. Chem. Theory Comput.* **2013**, *9*, 1600–1610.

(42) Gupta, P.; Teitel, S. Phase diagram of the two-dimensional lattice Coulomb gas. *Phys. Rev. B* **1997**, *55*, 2756–2759.

(43) Bair, S.; McCabe, C.; Cummings, P. T. Comparison of Nonequilibrium Molecular Dynamics with Experimental Measurements in the Nonlinear Shear-Thinning Regime. *Phys. Rev. Lett.* **2002**, *88*, 058302.

(44) Hu, H.-W.; Carson, G. A.; Granick, S. Relaxation time of confined liquids under shear. *Phys. Rev. Lett.* **1991**, *66*, 2758–2761.

(45) Cui, S. T.; McCabe, C.; Cummings, P. T.; Cochran, H. D. Molecular dynamics study of the nano-rheology of *n*-dodecane confined between planar surfaces. *J. Chem. Phys.* **2003**, *118*, 8941–8944.

(46) Kano, M.; Yasuda, Y.; Okamoto, Y.; Mabuchi, Y.; Hamada, T.; Ueno, T.; Ye, J.; Konishi, S.; Takeshima, S.; Martin, J. M.; Bouchet, M. I. D.; Mogne, T. L. Ultralow Friction of DLC in Presence of Glycerol Mono-Oleate. *Tribol. Lett.* **2005**, *18*, 245–251.

(47) Topolovec-Miklozic, K.; Lockwood, F.; Spikes, H. Behaviour of Boundary Lubricating Additives on DLC Coatings. *Wear* **2008**, *265*, 1893–1901.

(48) Minami, I.; Kubo, T.; Nanao, H.; Mori, S.; Sagawa, T.; Okuda, S. Investigation of Tribo-Chemistry by Means of Stable Isotopic Tracers, Part 2: Lubrication Mechanism of Friction Modifiers on Diamond-Like Carbon. *Tribol. Trans.* **2007**, *50*, 447–487.

(49) Costello, M. T. Effects of Basestock and Additive Chemistry on Traction Testing. *Tribol. Lett.* **2005**, *18*, 91–97.

(50) Murase, A.; Ohmori, T. A Systematic Density Functional Study of Fluorination in Methane, Ethane and Ethylene. *Surf. Interface Anal.* **2001**, *31*, 232–241.

(51) Shrestha, L. K.; Glatter, O.; Aramaki, K. Structure of Nonionic Surfactant Glycerol α-Monomyristate Micelles in Organic Solvents: A SAXS Study. *J. Phys. Chem. B* **2009**, *113*, 6290–6298.

(52) Shrestha, L. K.; Shrestha, R. G.; Abe, M.; Ariga, K. Reverse Micelle Microstructural Transformations Induced by Oil and Water. *Soft Matter* **2011**, *7*, 10017–10024.

(53) Shrestha, R. G.; Shrestha, L. K.; Ariga, K.; Abe, M. Reverse Micelle Microstructural Transformations Induced by Surfactant Molecular Structure, Concentration, and Temperature. *J. Nanosci. Nanotechno.* **2011**, *11*, 7665–7675.

(54) Shrestha, L. K.; Shrestha, R. G.; Aramaki, K.; Hill, J. P.; Ariga, K. Nonionic Reverse Micelle Formulation and Their Microstructure Transformations in an Aromatic Solvent Ethylbenzene. *Colloids Surf. A* **2012**, *414*, 140–150.

(55) Bradley-Shaw, J. L.; Camp, P. J.; Dowding, P. J.; Lewtas, K. Glycerol Monooleate Reverse Micelles in Nonpolar Solvents: Computer Simulations and Small-Angle Neutron Scattering. *J. Phys. Chem. B* **2015**, *119*, 4321–4331.

(56) Jabbarzadeh, A.; Tanner, R. I. Thin Lubricant Films Confined Between Crystalline Surfaces: Gold Versus Mica. *Tribol. Int.* **2011**, *44*, 711–719.

(57) Bhandary, D.; Khan, S.; Singh, J. K. Structure and Dynamics of *n*-Alkanol Monolayers on a Mica Surface. *J. Phys. Chem. C* **2014**, *118*, 6809–6819.

(58) Das, J.; Eun, C.; Perkin, S.; Berkowitz, M. L. Restructuring of Hydrophobic Surfaces Created by Surfactant Adsorption to Mica Surfaces. *Langmuir* **2011**, *27*, 11737–11741.

(59) LAMMPS Molecular Dynamics Simulator. http://lammps.sandia.gov.

(60) Plimpton, S. Fast Parallel Algorithms for Short-Range Molecular Dynamics. *J. Comp. Phys.* **1995**, *117*, 1–19.

(61) Heinz, H.; Castelijns, H. J.; Suter, U. W. Structure and Phase Transitions of Alkyl Chains on Mica. *J. Am. Chem. Soc.* **2003**, *125*, 9500–9510.

(62) Heinz, H.; Suter, U. W. Surface Structure of Organoclays. *Angew. Chem. Int. Ed.* **2004**, *116*, 2289–2293.

(63) Heinz, H.; Koerner, H.; Anderson, K. L.; Vaia, R. A.; Farmer, B. L. Force Field for Mica-Type Silicates and Dynamics of Octadecylammonium Chains Grafted to Montmorillonite. *Chem. Mater.* **2005**, *17*, 5658–5669.

(64) Heinz, H.; Lin, T.-J.; Mishra, R. K.; Emami, F. S. Thermodynamically Consistent Force Fields for the Assembly of Inorganic, Organic, and Biological Nanostructures: The INTERFACE Force Field. *Langmuir* **2013**, *29*, 1754–1765.

(65) Martínez, L.; Andrade, R.; Birgin, E. G.; Martínez, J. M. PACKMOL: A Package for Building

Initial Configurations for Molecular Dynamics Simulations. *J. Comp. Chem.* **2009**, *30*, 2157–2164.

(66) Dieterich, J. H. Modeling of Rock Friction .1. Experimental Results and Constitutive Equations. *J. Geophys. Res.* **1979**, *84*, 2161–2168.

(67) Dieterich, J. H. Modeling of Rock Friction .2. Simulation of Pre-Seismic Slip. *J. Geophys. Res.* **1979**, *84*, 2169–2175.

(68) Ruina, A. Slip Instability and State Variable Friction Laws. *J. Geophys. Res.* **1983**, *88*, 359–370.

(69) Gu, J. C.; Rice, J. R.; Ruina, A. L.; Tse, S. T. Slip Motion and Stability of a Single Degree of Freedom Elastic System With Rate and State Dependent Friction. *J. Mech. Phys. Sol.* **1984**, *32*, 167–196.

(70) Briscoe, B. J.; Evans, D. C. B. The Shear Properties of Langmuir-Blodgett Layers. *Proc. R. Soc. Lond. A* **1982**, *380*, 389–407.

(71) Perez, D.; Dong, Y.; Martini, A.; Voter, A. F. Rate Theory Description of Atomic Stick-Slip Friction. *Phys. Rev. B* **2010**, *81*, 24515.

(72) Leng, Y. S.; Cummings, P. T. Fluidity of Hydration Layers Nanoconfined between Mica Surfaces. *Phys. Rev. Lett.* **2005**, *94*, 026101.

(73) Cui, S. T.; Cummings, P. T.; Cochran, H. D. Molecular simulation of the transition from liquidlike to solidlike behavior in complex fluids confined to nanoscale gaps. *J. Chem. Phys.* **2001**, *114*, 7189–7195.

(74) Yue, D.-C.; Ma, T.-B.; Hu, Y.-Z.; Yeon, J.; van Duin, A. C. T.; Wang, H.; Luo, J. Tribochemistry of Phosphoric Acid Sheared between Quartz Surfaces: A Reactive Molecular Dynamics Study. *J. Phys. Chem. C* **2013**, *117*, 25604–25614.

(75) Erbaş, A.; Horinek, D.; Netz, R. R. Viscous Friction of Hydrogen-Bonded Matter. *J. Am. Chem. Soc.* **2012**, *134*, 623–630.

Graphical TOC Entry